

Numerical Simulation of Flow around a Waterjet Propelled Ship

Takanori Hino¹, Kunihide Ohashi¹

¹National Maritime Research Institute, Tokyo, Japan

ABSTRACT

Waterjet propulsion systems are widely used as a propulsor of high speed vessels. In order to design a ship with a waterjet system, estimation of its hydrodynamic performance is crucial. However, it is rather difficult to analyze propulsive performance of a waterjet ship even by tank tests due to the complexity of the system. CFD(Computational Fluid Dynamics) is expected to be an effective tool for analyzing hydrodynamic performance of such a complex system. In the present paper, CFD analysis is applied to free surface flow around a waterjet propelled ship. A waterjet propulsor is implemented as an actuator disk model placed inside a duct. Flow computations are performed in the conditions with and without waterjet operation. Also computed is a flow around a bare hull without a duct. Results are compared with one another and effects of a waterjet duct and a waterjet propulsor to flow fields are discussed. Finally thrust analysis based on the momentum flux difference is applied to simulated flow field and the applicability of CFD method to performance evaluation of a waterjet propelled ship is demonstrated.

Keywords

Waterjet, Computational Fluid Dynamics, High Speed Vessel

1 INTRODUCTION

Waterjet propulsion systems are widely used as a propulsor of high speed vessels (Allison, 1993). In order to design a ship with a waterjet system, it is important to estimate its hydrodynamic performance. However, since a waterjet propulsion system has many components such as an inlet, a duct, an impeller and a nozzle and they interacts with a ship hull in a complicated manner, it is rather difficult to analyze propulsive performance of a waterjet ship even by tank tests.

CFD(Computational Fluid Dynamics) is expected to be an effective tool for analyzing performance of such a complex system. It provides not only hydrodynamic forces of a hull but also a detailed flow field data, which is essential for the estimation of a waterjet performance evaluation.

A number of CFD applications have been reported for the simulations of a waterjet duct flow, such as (Turnock et al., 1997), (Bulten, 2006), (Hino, 2007), in which interactions

between a duct and a impeller are studied. Furthermore, a waterjet-hull interaction problems are also analyzed by CFD (Ebert et al., 2003), although free surface effects are not taken into account there.

In the present paper, CFD analysis of a free surface flow around a waterjet propelled ship is performed. Flows around a high-speed ship in the conditions with and without waterjet operation are computed using a Navier-Stokes solver. For towed condition, flows around a bare hull without a duct and around a hull with a duct are also computed. These results are compared with one another and effects of a waterjet duct and a waterjet propulsor to flow fields are discussed. Finally, the area upstream of the duct intake from where the flow goes into the intake (the capture area) is numerically estimated from the computed flow field and a thrust analysis based on the momentum flux difference is applied. Through these analyses, the applicability of CFD method to performance evaluation of a waterjet propelled ship is demonstrated.

2 CFD Method

2.1 Bulk Flow Solver

The flow solver used in this study is called *SURF* ("Solution algorithm for Unstructured RaNS with FVM"). It is developed at National Maritime Research Institute (Hino, 1997, 1998). The governing equations are the three-dimensional Reynolds averaged Navier-Stokes equations for incompressible flows. In order to couple pressure with a velocity field, artificial compressibility concept is introduced into the continuity equation at the expense of time accuracy, which means that the present formulation is for a steady state solution. The equations can be written in a vector form as follows:

$$\frac{\partial \mathbf{q}}{\partial t} + \frac{\partial(\mathbf{e} - \mathbf{e}^v)}{\partial x} + \frac{\partial(\mathbf{f} - \mathbf{f}^v)}{\partial y} + \frac{\partial(\mathbf{g} - \mathbf{g}^v)}{\partial z} = 0 \quad (1)$$

where

$$\mathbf{q} = [p \quad u \quad v \quad w]^T$$

In the above expressions all the variables are made dimensionless using the reference density ρ_0 , velocity U_0 and length L_0 . For a free surface flow, pressure p is modified as

$$p = p^* + \frac{z}{F_n^2}$$

where p^* is the original pressure and F_n is the Froude number, $U_0/\sqrt{gL_0}$, with z being the vertical coordinate. By this modification of pressure, the gravitational acceleration term can be dropped from the z -momentum equations. The velocity components in the (x, y, z) direction is expressed as (u, v, w) .

The inviscid fluxes \mathbf{e} , \mathbf{f} and \mathbf{g} are defined as

$$\mathbf{e} = \begin{bmatrix} \beta u \\ u^2 + p \\ uv \\ uw \end{bmatrix}, \quad \mathbf{f} = \begin{bmatrix} \beta v \\ vu \\ v^2 + p \\ vw \end{bmatrix}, \quad \mathbf{g} = \begin{bmatrix} \beta w \\ wu \\ wv \\ w^2 + p \end{bmatrix}$$

where β is a parameter for artificial compressibility. The viscous fluxes \mathbf{e}^v , \mathbf{f}^v and \mathbf{g}^v are written as:

$$\mathbf{e}^v = \begin{bmatrix} 0 \\ \tau_{xx} \\ \tau_{xy} \\ \tau_{xz} \end{bmatrix}, \quad \mathbf{f}^v = \begin{bmatrix} 0 \\ \tau_{xy} \\ \tau_{yy} \\ \tau_{yz} \end{bmatrix}, \quad \mathbf{g}^v = \begin{bmatrix} 0 \\ \tau_{xz} \\ \tau_{yz} \\ \tau_{zz} \end{bmatrix}$$

where

$$\tau_{ij} = \left(\frac{1}{R_n} + \nu_t \right) \left(\frac{\partial u_i}{\partial x_j} + \frac{\partial u_j}{\partial x_i} \right)$$

and R_n is the Reynolds number defined as $U_0 L_0 / \nu$ with ν being the kinematic viscosity. ν_t is the non-dimensional kinematic eddy viscosity determined by a turbulence model.

Since a numerical procedure for the Navier-Stokes equations are described in (Hino, 1997, 1998), only the brief outline is given here.

Spatial discretization is based on a cell-centered finite-volume method. A computational domain is divided into unstructured polyhedral cells and flow variables (pressure, velocity and eddy viscosity) are stored in the center of each cell. Cells whose shape is hexahedra, tetrahedra, prisms or pyramids can be used and the combinations of these cells give greater flexibility for handling complex geometry.

For the inviscid fluxes (convection terms and pressure gradient terms), the second order upwind scheme based on the flux-differencing splitting of Roe (Roe, 1986) with the MUSCL approach is employed. The viscous fluxes are evaluated by the second order central scheme. Thus, the overall accuracy in space is second order.

The backward Euler scheme is used for the time integration. Local time stepping method is used, in which time increment is determined for each cell in such a way that the CFL number is globally constant. The linear equations derived from the time linearization of the fluxes are solved by the Symmetric Gauss-Seidel (SGS) iteration. Finally, the multigrid method is employed for convergence acceleration.

The turbulence models implemented are the one-equation model by Spalart and Allmaras (Spalart and Allmaras, 1994) and its variant (Rhee and Hino, 2000) which is tuned for ship wake prediction.

2.2 Free Surface Treatment

Free surface is an interface between air and water in the present applications. Free surface conditions consist of kinematic and dynamic conditions and they are implemented in the interface capturing framework.

The kinematic condition is the condition that fluid particles on a free surface remain on an interface. This is written in a mathematical form as follows:

$$\frac{DH}{Dt} = \frac{\partial H}{\partial t} + u \frac{\partial H}{\partial x} + v \frac{\partial H}{\partial y} + w \frac{\partial H}{\partial z} = 0 \quad (2)$$

where a free surface shape is defined as

$$H(x, y, z; t) = 0$$

In the present scheme, this kinematic condition is formulated based on the localized level set method (Peng et al., 1999) which improves the efficiency of the original level set approach (Sussman et al., 1994). The brief description of the implementation is presented in the following. The detail can be found in (Hino, 1999) and (Hino, 2004).

The level set function ϕ is defined as the signed distance from the interface and have the positive and negative values correspond to water and air regions, respectively. Since $\phi(x, y, z; t) = 0$ defines the free surface shape, the kinematic condition can be satisfied if the following equation is used to update ϕ :

$$\frac{D\phi}{Dt} = \frac{\partial \phi}{\partial t} + u \frac{\partial \phi}{\partial x} + v \frac{\partial \phi}{\partial y} + w \frac{\partial \phi}{\partial z} = 0 \quad (3)$$

In the localized version of the level set method, the two parameters γ_1 and γ_2 where $0 < \gamma_1 < \gamma_2$ are introduced. The signed distance function is rewritten as $d(x, y, z; t)$ and the definition of the level set function is modified as

$$\phi = \begin{cases} \gamma_1 & \text{if } d > \gamma_1 \\ d & \text{if } |d| \leq \gamma_1 \\ -\gamma_1 & \text{if } d < -\gamma_1 \end{cases} \quad (4)$$

Thus, the level set function is localized within the bandwidth $2\gamma_1$ from the interface. The transport equation (3) is also modified as

$$\frac{\partial \phi}{\partial t} + C(\phi) \left(u \frac{\partial \phi}{\partial x} + v \frac{\partial \phi}{\partial y} + w \frac{\partial \phi}{\partial z} \right) = 0 \quad (5)$$

where $C(\phi)$ is the cut-off function whose value is unity within the band ($|\phi| \leq \gamma_1$) and varies smoothly to zero in the region $\gamma_1 < |\phi| \leq \gamma_2$ and fixed to be zero in the outside ($|\phi| > \gamma_2$). In this way, the update of ϕ is performed only in the region where $|\phi| < \gamma_2$. The numerical solution method for Eq.(5) is similar to the flow equations. The cell centered finite-volume is applied for the spatial discretization and the time integration is carried out by the Euler backward scheme.

In order to avoid reflection of free surface waves in the outer boundaries of a computational domain, the wave

damping method (Hino, 1999) is used. Also, there is a singular behavior of the interface in the region close to a solid wall. The no-slip condition imposed on a solid wall prevents the interface movement there, while the interface in the outer region moves due to the fluid motion. It causes the unphysical large deformation of ϕ near a solid wall. The extrapolation approach is employed here to solve this problem, in which the value of ϕ for the cells close to the wall is extrapolated from the outer cell. The selection of outer cells on unstructured grids also needs special attention (Hino, 1999). The re-initialization of the level set is an important step in the level set method, since the level set function is no longer a distance function after the convection. The re-initialization process can be done using the partial differential equation as in (Sussman et al., 1994) or (Peng et al., 1999).

Since most of ship hydrodynamics applications require a flow field of water region only, single-phase flow approach is used (Hino, 1999), i.e., flow variables in the air region are extrapolated from a water region in such a way that the dynamic condition on free surface boundary is satisfied. This method also has an advantage that it is not necessary to cope with large density difference between air and water. The dynamic free surface conditions can be approximated by the following two conditions. First, the velocity gradients normal to the free surface are zero. Second, the pressure on the free surface is equal to atmospheric pressure. In order to satisfy the first condition, the velocity components are extrapolated from the water region to the air region in the direction normal to the interface. Following the localized level set method (Peng et al., 1999), this is achieved by solving the following equation in the air region where $\phi < 0$ with the pseudo time τ .

$$\frac{\partial \mathbf{q}}{\partial \tau} - \frac{\nabla \phi}{|\nabla \phi|} \cdot \nabla \mathbf{q} = 0 \quad (6)$$

Note that the quantity $-\nabla \phi / |\nabla \phi|$ is the unit vector normal to the interface whose direction is from water to air. In the region away from the interface where ϕ is constant, $-\nabla \phi / |\nabla \phi|$ is replaced by the vector $(0, 0, 1)$.

The pressure boundary condition is written as

$$p = \frac{h}{F_n^2} \text{ on the free surface} \quad (7)$$

where atmospheric pressure is assumed to be zero and h is the z -coordinate of the interface. For an air cell which is next to a water cell, pressure is extrapolated in such a way that the pressure on a free surface between two cells has the value of Eq.(7). In case that an air cell has several adjacent water cells, the pressure value is obtained by taking the average of the extrapolated values from each water cell. In the remaining air region, pressure is extrapolated using Eq.(6).

2.3 Waterjet propulsor model

The purpose of self-propulsion tests is to acquire self-propulsion factors, such as thrust deduction or wake fraction. Unlike a conventional propulsion system, a waterjet propulsor is integrated into a ship hull and interaction between a hull and a propulsor is more complicated.

For a self-propulsion simulations using CFD, a waterjet propulsor model should be implemented in a flow solver. An actuator model is introduced for the present study, in which a waterjet duct geometry is modeled in a computational grid. An actuator disk is placed at the impeller position inside a duct and a body force is added in a computational cells which intersect with an actuator disk. The body force is assumed to be distributed uniformly on a actuator disk and only the force component normal to the disk is considered for simplicity.

3 RESULTS AND DISCUSSION

3.1 Ship Model and Computational Conditions

A ship model used is a high-speed boat of 30.5 m long which is equipped with twin waterjet propulsors. A series of model tests have been carried out including resistance and self-propulsion tests with a model of 1/10 scale.

The Froude number and the Reynolds number of computations are about 1.0 and 10^6 , respectively. Note that the Reynolds number is selected based on the convenience of grid generation and it does not match the experimental condition.

Although the flow solver has a capability for estimating trim and sinkage of a ship in a running condition, the attitude of a ship measured in the model test is given and fixed in the present computations. The trim $((d_a - d_f)/L_{pp})$ is 0.0446 and the sinkage $((d_a + d_f)/2L_{pp})$ is -0.0108, where d_a and d_f is dipping at AP and FP, respectively.

The computational grid is generated using the commercial grid generation software Gridgen. Two grids are prepared; one for the bare hull without a waterjet duct and the other is a hull with a duct. Both grids are based on multiblock structured grids covering only the port side of a domain assuming y -symmetry.

The grids are generated around a ship in an even-keel condition and then the grid morphing module of the flow solver is used to obtain the grids around a ship with trim and sinkage.

The grid in the case with a duct is generated first and the bare hull grid is obtained by removing a duct block. Thus, the grid blocks around a main hull are identical for both grids. The blocks around a ship consists of $97 \times 81 \times 65$ points and its topology is an O-O type. In the case with a duct, additional block with $17 \times 17 \times 65$ points is placed inside a duct. Note that a waterjet impeller/stator, shaft and nozzle geometries are not included in the grid for simplicity and the waterjet impeller is modeled by an actuator disk model as described earlier.

Since the ship speed is quite high and the wave length of generated waves becomes long, the computational domain is set larger than that of the conventional mid-speed applications. The domain size is

$$-4 \leq x/L_{pp} \leq 5, \quad -4.5 \leq y/L_{pp} \leq 0,$$

$$-4.42 \leq z/L_{pp} \leq 0.115$$

where the ship is placed between $0 \leq x \leq 1$. Although the averaged minimum spacing near the ship hull is 1.0×10^{-5} and sufficiently small for resolving the boundary layer on a hull surface, the minimum spacing on the duct wall is two orders of magnitude larger and the boundary layer resolution cannot be expected on the duct wall. The total view of the grid is shown in Fig. 1 and the bow and stern views are shown in Fig. 2.

The turbulence model used is Spalart-Allmaras model and flow fields are assumed to be fully turbulent.

Three computations are carried out. The first one is for a bare hull in a towing condition(abbreviated as “TOW-BARE”), the second is for a hull with a duct also in a towing condition(“TOW-DUCT”) and the last one is a self-propulsion condition with a hull with a duct configuration(“PROP-DUCT”).

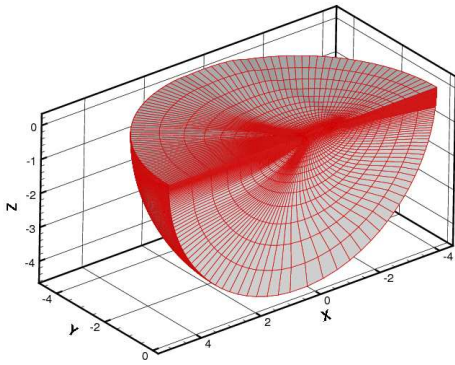
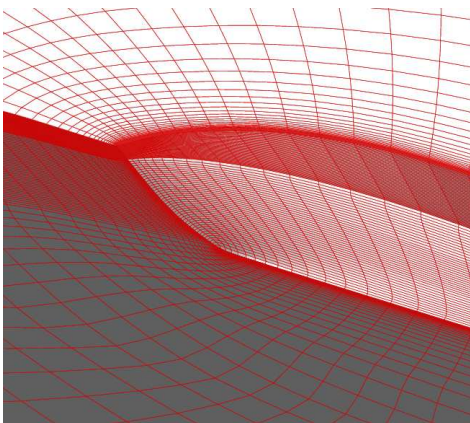
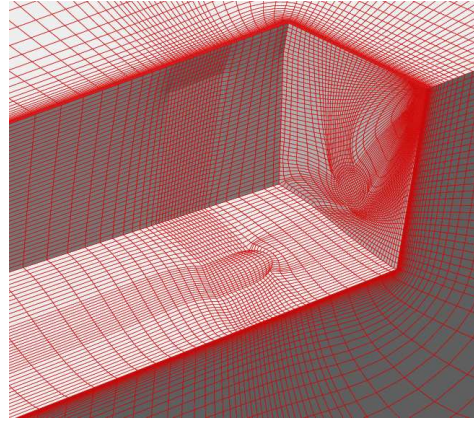


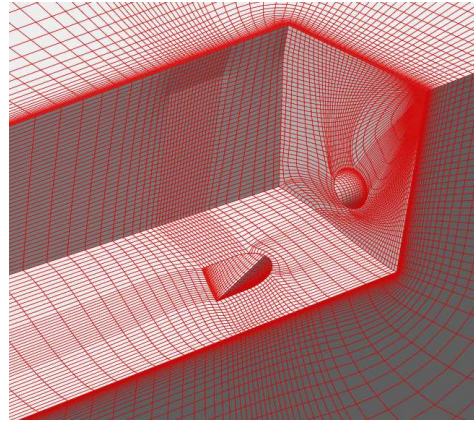
Fig.1 Computational grid (total view).



(a) Bow view



(b) Stern view (a bare hull)



(c) Stern view (a hull with a duct)

Fig.2 Computational grids: (a) Bow view, (b) stern view of a bare hull grid and (c) stern view of a grid with a duct.

3.2 Flow fields

The computed wave patterns are shown in Figs.3. The Froude number is so high (around 1.0) that the ship is in a planing condition. The so-called “rooster tail” waves are generated behind a transom stern of a ship. The waterjet can be observed in the “PROP-DUCT” condition where the actuator disk accelerates the flow inside the duct. It is interesting that the flow comes out from the outlet in the “TOW-DUCT” condition as well as “PROP-DUCT”.

Figs.4 depict the comparisons of the computed wave contours among three conditions. The bow wave of “PROP-DUCT” is smaller than that of two towing conditions. On the other hand, the stern wave is larger in the “TOW-BARE” than in the “TOW-DUCT” or “PROP-DUCT” conditions. Note that the attitude of a ship is identical among three conditions, while actually the change of wave fields affect the trim and sinkage of a ship and vice versa.

Fig.5 is the magnified view of the wave contours in the stern region for the “TOW-DUCT” and “PROP-DUCT” conditions. The difference of jet flows between towing and self-propelled conditions can be observed clearly.

The comparisons of hull surface pressure distribution are shown in Figs.6. With the operation of the waterjet propulsor, the low pressure zone of the aft bottom increases and the high pressure zone in the fore part is reduced, which

corresponds to the smaller bow wave in the self-propelled condition observed in Figs.4.

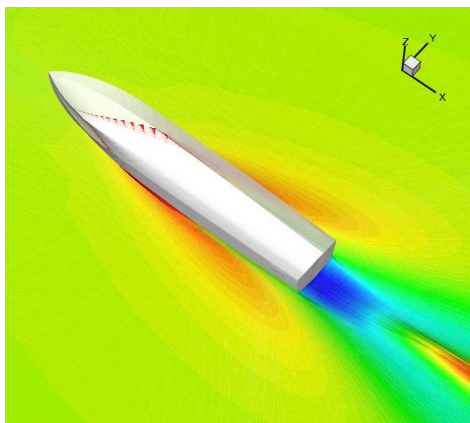
Figs.7 show the pressure distributions in the duct center plane for the “TOW-DUCT” and “PROP-DUCT” conditions. High pressure in the lip of the duct inlet and the low pressure in the fore edge of the inlet can be observed in both plots, although the peak values are larger in the “PROP-DUCT” condition. Due to the suction of the impeller, pressure inside the duct is lower in the “PROP-DUCT” case. Also seen is the pressure jump in the impeller position in the “PROP-DUCT” plot due to the body force. The shape of jet flows is thicker in the “PROP-DUCT” than in the “TOW-DUCT” due to the momentum given by the propulsor.

Shown in Figs.8 are the contours of u velocity for three conditions at the section close to the aft-end. The boundary layer on the bottom in the “TOW-BARE” condition develops along the wall, since the hull geometry is smooth and a ship is planing. In case of “TOW-DUCT”, the boundary layer on the bottom becomes thinner behind a duct inlet due to the suction effect. This trend is pronounced in the “PROP-DUCT” condition, since the suction effect is stronger due to the propulsor operation. The velocity in the duct is higher in the “PROP-DUCT” condition and the maximum value is about 1.8 times larger than the ship speed.

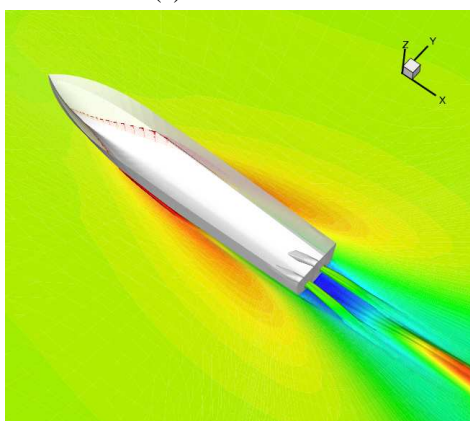


(c) PROP-DUCT

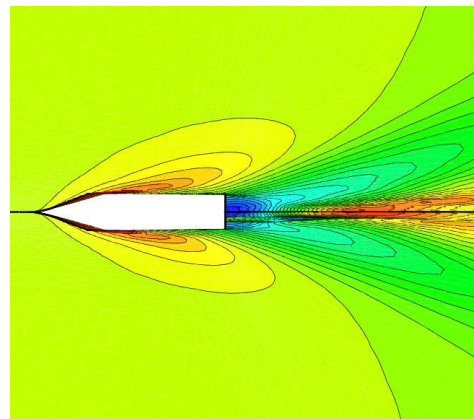
Fig.3 Computed wave patterns: (a) TOW-BARE, (b) TOW-DUCT and (c) PROP-DUCT.



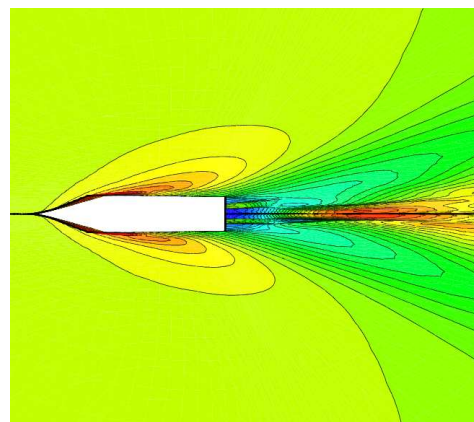
(a) TOW-BARE



(b) TOW-DUCT



(a) Top: TOW-BARE bottom: PROP-DUCT



(b) Top: TOW-DUCT bottom: PROP-DUCT

Fig.4 Comparisons of computed wave contours: (a) TOW-BARE and PROP-DUCT, (b) TOW-DUCT and PROP-DUCT.

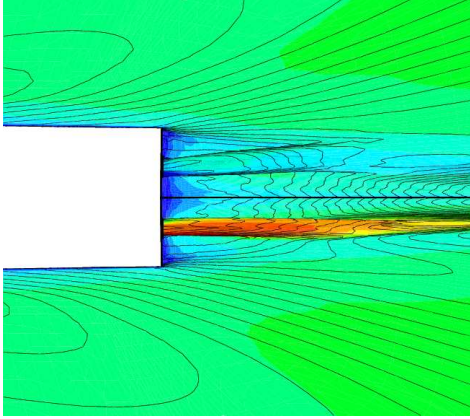
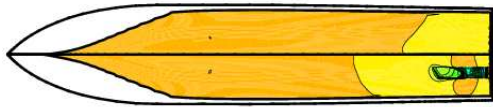
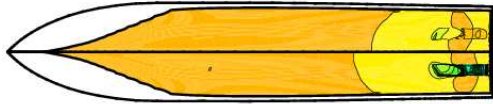


Fig.5 Comparisons of computed wave contours in the stern: top TOW-DUCT, bottom PROP-DUCT.

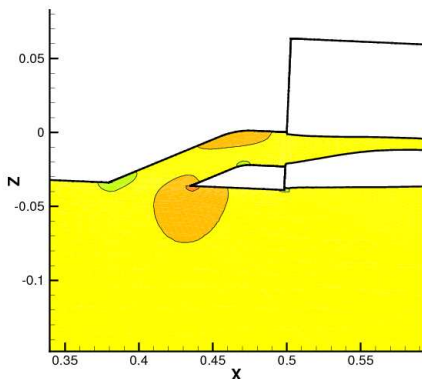


(a) Top: TOW-BARE bottom: PROP-DUCT

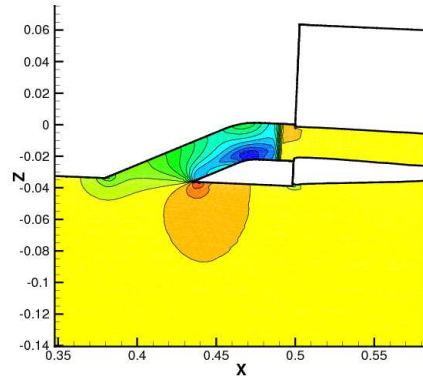


(b) Top: TOW-DUCT bottom: PROP-DUCT

Fig.6 Comparisons of hull surface pressure(bottom view): (a) TOW-BARE and PROP-DUCT, (b) TOW-DUCT and PROP-DUCT.



(a) TOW-DUCT



(b) PROP-DUCT

Fig.7 Comparisons of pressure distributions in the duct center plane : (a) TOW-DUCT, (b) PROP-DUCT.

3.3 Propulsive performance estimation

The computed hydrodynamic forces are tabulated in Table 2. Note that in the “PROP-DUCT” condition, the amount of body force at the actuator disk is given based on the estimated thrust force, which is $T/0.5\rho U^2 S = 11.15 \times 10^{-3}$. The actual gross thrust force is determined from the momentum flux difference between the nozzle exit and the upstream of the duct inlet and cannot be determined beforehand. Therefore the horizontal force balance is not achieved in the present computation.

Gross thrust force can be estimated as

$$T_g = Q(V_j - V_m) \quad (8)$$

where Q is the flow rate at a duct section and V_j and V_m are the jet velocity and the momentum velocity, respectively. V_j is the average velocity at the duct exit and the numerical integration of the computed result gives the value of 1.48 (nondimensionalised by U) and $Q/UL^2 = 6.17 \times 10^{-4}$. Note that the nozzle shape is not modeled in the present configuration and the actual jet velocity may be larger than this value.

The momentum velocity V_m is the average velocity of the capture area. The capture area is the area upstream of the duct intake from where the flow goes into the intake. It is difficult to determine this capture area by experiment. Since CFD simulations provide the detailed flow field data, the capture area can be estimated more easily.

Fig.9 is the limiting streamlines of both “TOW-BARE” and “PROP-DUCT” conditions on a ship bottom. While the streamlines of “TOW-BARE” are almost straight, “PROP-DUCT” result shows the deformed streamlines. The back-trace of the streamlines coming into the intake shows the width of the capture area is as twice as wide as that of the intake duct. This is a little bit larger than the value of the recommended procedure of ITTC(International Towing Tank Conference) (ITTC, 2005) which is 1.5 times the duct width. The capture area sections is set at one impeller

diameter upstream of the duct edge and the height of the capture area is determined in such a way that the flow rate of the capture area is equal to the flow rate of the duct exit, where the shape of the capture area is assumed to be an ellipse.

Fig. 10 shows the estimated capture area. Also plotted are the streamlines which go through near the inner edge of the duct intake. The streamlines are passing near the edge of estimated capture area and the estimated capture area appears to be consistent with the flow field.

The momentum velocity V_m is computed as 0.96. Thus the gross thrust force is

$$T_g/0.5\rho U^2 S = 6.42 \times 10^{-4}$$

Since the hull resistance of the “PROP-DUCT” condition is 9.71×10^{-3} , the thrust is too small for the force balance. However, as mentioned above, the actual jet velocity may be larger and therefore the present thrust may be underestimated to some extent. In order to adjust the thrust force automatically for the force balance, the procedure for estimating a capture area and momentum velocity described above should be implemented in the flow solver.

Table 2 Computed hydrodynamic forces

Condition	$Ct \times 10^3$	$Cf \times 10^3$	$Cr \times 10^3$
TOW-BARE	8.93	5.21	4.52
TOW-DUCT	10.27	5.66	5.86
PROP-DUCT	9.71	6.03	5.30

$C_* = R_*/0.5\rho U^2 S$, where S is the wetted surface area with a running trim.

$Cr = Ct - Cf0$, $Cf0$ is the value of Schoenherr line.

4 CONCLUSIONS

The CFD method is applied to the hydrodynamic performance analysis of a waterjet propelled ship. The waterjet duct is modeled in a computational grid and an actuator disk model is used to account for the impeller effect. The actuator force is given based on the estimated thrust.

Free surface flows around a bare hull and a hull with a duct both in towed and self-propelled conditions are computed. The levelset approach of free surface modeling successfully captures the features of wave generation of a planing boat and the jet flows behind the duct outlet.

The pressure distributions on a ship hull and inside a waterjet duct are compared with one another and the effects of a waterjet propulsor to flow fields are visualized.

The capture area needed to thrust force evaluation is estimated using the computed flow field. It is shown that the estimated capture area is consistent with the streamlines going through the duct inlet. Finally, the thrust force is computed by the momentum flux difference between the capture area and the waterjet outlet. By using this thrust evaluation procedure, the self-propulsion point can

be searched automatically during the computation and the usability of the method will be enhanced in the future.

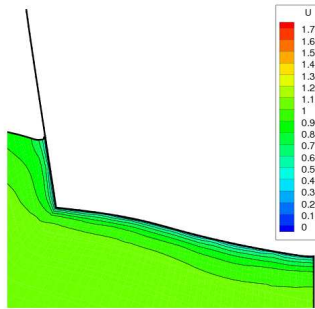
This study is conducted with the support by Grant-in-Aid for Scientific Research (A) 18360425 from Japan Society for the Promotion of Science. Additional support is provided by the cooperative study between Japan Coast Guard and National Maritime Research Institute.

REFERENCES

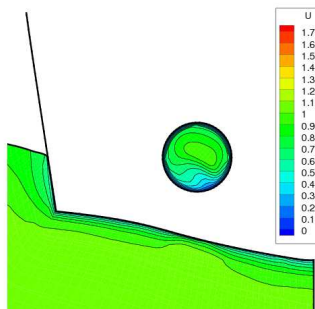
- Allison, J. (1993). 'Marine Waterjet Propulsion'. SNAME Transaction, 275:335 – 101.
- Turnock, S.R. et al. (1997). 'Investigation of Hull-Waterjet Flow Interaction'. In Proc. 4th Intern. Conf. Fast Sea Transportation.(Fast '97).
- Bulten, N.W.H. (2006). 'Numerical Analysis of Waterjet Propulsion System'. PhD thesis, Technical University of Eindhoven.
- Hino, T. (2007). 'Numerical Simulation of Waterjet Duct Flow'. CFD in Ship Design, Hamburg, Schiffbautechnische Gesellschaft e.V.
- Ebert, M.P., Gorski, J.J. and Coleman, R.M. (2003). 'Viscous Flow Calculations of Waterjet Propelled Ships. In Proc. 8th Intern. Conf. on Numerical Ship Hydro., Busan, Korea.
- Hino, T. (1997). 'A 3D Unstructured Grid Method for Incompressible Viscous Flows'. J. of the Soc. Naval Archit. Japan, 182:9 –15.
- Hino T. (1998). 'Navier-Stokes Computations of Ship Flows on Unstructured Grids'. In Proc. of the 22nd Symp. on Naval Hydro, Washington DC, USA.
- Roe, P.L. (1986). 'Characteristic-Based Schemes for the Euler Equations'. Ann. Rev. Fluid Mech., 18:337 – 365.
- Spalart, P.R. and Allmaras, S.R. (1994). 'A One-Equation Turbulence Model for Aerodynamic Flows'. La Recherche Aéropatiale, 1:5 – 21.
- Rhee, S.H. and Hino, T. (2000). 'Unstructured Grid Flow Solver for Practical Ship Hulls'. In Proc. Workshop in Numerical Ship Hydrodynamics, Gothenburg, Sweden.
- Peng, D., Merriman, B., Osher, S., Zhao, H. and Kang, M. (1999). 'A PDE-Based Fast Localized Level Set Method'. J. Comput. Phys., 410:438 – 155.
- Sussman, M., Smereka, P. and Osher, S.(1994). 'A Level Set Approach for Computing Solutions to Incompressible Two-Phase Flow'. J. Comput. Phys., 146:159 – 114.
- Hino, T. (1999). 'An Interface Capturing Method for Free Surface Flow Computations on Unstructured Grids'. J. of the Soc. Naval Archit. Japan, 186:177 – 183.

Hino, T. (2004). 'Numerical Simulations of Breaking Waves around an Advancing Ship by an Unstructured NS Solver'. In Proc. of the 25th Symp. on Naval Hydro.

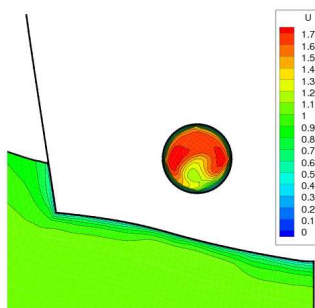
24th ITTC Specialsit Committee on Validation of Waterjet Test Procedures (2005). 'Final Report and Recommendations to 24th ITTC'. In Proc. 24th Intern. Towing Tank Conf.



(a) TOW-BARE



(b) TOW-DUCT



(c) PROP-DUCT

Fig.8 Computed wake distribution at $x/LPP = 0.4975$: (a) TOW-BARE, (b) TOW-DUCT and (c) PROP-DUCT.

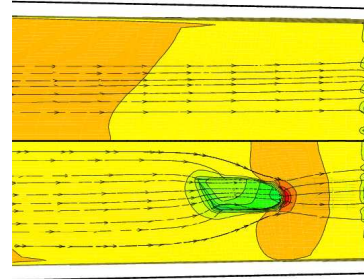
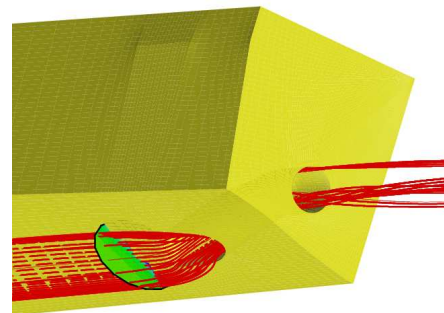
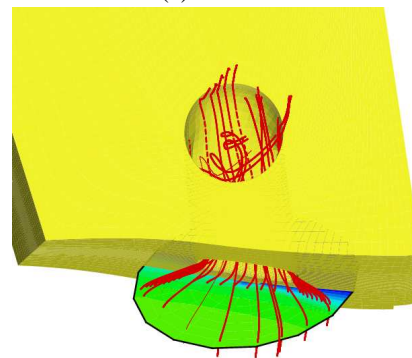


Fig.9 Comparison of limiting streamlines on a ship bottom, top: TOW-BARE, bottom: PROP-DUCT.



(a) Side view



(b) Rear view

Fig.10 Estimated capture area and streamlines